Investigating the transition from Molecular Dynamics to Smoothed Particle Hydrodynamics

PH3110

Royal Holloway University of London

Ioannis Nikiteas

Supervisor: Professor David M. Heyes

March 16, 2017

Abstract

Molecular dynamics (MD) and Smoothed particle hydrodynamics (SPH) are fluid models used to describe systems of different, lengths and time scales. With the former referring to microscopic regimes and the latter modelling mesoscopic fluids. The objective of this report is to investigate, whether a continuous transition can be achieved, in an isothermal container, by altering the softness parameters of a modified, only-repulsive Lennard-Jones potential. Results from the simulations show two prominent fluid regimes, MD, for highly repulsive pair potentials and weak-interactions regime, for weak particle coupling. SPH is bounded by the two regimes and it is only observed for limited values of the system parameters. Moreover, for parameters assigned to the SPH regime, coarse-graining of the fluid is observed while for the weak-interactions region micro-clusters of particles are detected. We show for a fluid in the weak-interactions regime, the system will never diffuse nor decorrelate from its initial conditions. Interestingly, we observed multiple isosbestic points in the microscopic density analysis of the system, for an increasing potential strength parameter.

Contents

I. INTRODUCTION

This report will examine the individual properties of two different models which are commonly used to describe systems of fluids, the Molecular Dynamics model, MD, and the (simplified) Smooth Particle Hydrodynamics model, SPH. The former, MD, uses the classical equations of motion (Newton's equations) to simulate the time evolution of a N-body particle system, where the forces acting on each particle depend on a well defined interatomic potential [1],[2]. The particles' potentials interact with the surrounding potentials of neighbouring particles resulting into a fluid where its particles are correlated in an atomic level. The latter, SPH, is a mesh-free particle simulation method used to solve fluid mechanics problems in a mesoscopic regime. The particles are smoothly distributed in space and are described by a kernel (weighting) function, which acts as a simplifying mechanism for the spatial derivatives resulting into ordinary differential equations for the time development of the system [3], [4].

The main focus of this paper is to simulate the transition between MD and SPH using a computer simulation program written in C++. Initially, the MD system was formed and then by smoothing the pair potentials of the particles, it was tested if the resulting system had been coarse-grained. Coarse-graining would imply a uniform kernel function acting on the fluid and hence a successful transition to the SPH regime. The C++ simulation, monitored and calculated various quantities of the system, including the positions, velocities and accelerations, kinetic and potential energies per particle along with their pressures and some properties providing insights for the structure of the fluid, such as radial distribution function, mean square displacement and velocity autocorrelation function.

II. THEORETICAL BACKGROUND

A. Relation of Molecular Dynamics to Smooth Particle Hydrodynamics

The simulations are based on a MD model using Newton's law for acceleration $F = m\ddot{x}$. Initially, the liquid was placed in a simple cubic lattice structure and then random velocities were assigned to each individual particle. The particles interacted in pairs using a modified, only repulsive, Lennard-Jones pair potential from Equation(1) and had forces described by Equation (2). Where ε and σ are chosen to be 1 to simplify the calculations, $\mathbf{r}$ is the relative position vector of the particle pair ij, n characterises the strength of the potential and A is the softness parameter of the potential, one of the predominant focus points of the report.

$$\phi_{ij}(r) = \varepsilon\left(\frac{\sigma}{(r^2 + A)}\right)^{\frac{n}{2}} \tag{1}$$

$$\mathbf{f}_i = -\nabla\Phi = \frac{1}{N}\sum_{i=1}^{N}\sum_{i<j} n\mathbf{r}_{ij}\frac{1}{\left(r_{ij}^2 + A\right)^{n/2-1}} \tag{2}$$

On the other hand, SPH is characterised by the partial differential equations of conservation for continuity, motion and energy, of a continuum fluid [5]. Where Equation (3), written in its Lagrangian derivatives, describes a "smoothed", uniformly distributed system with mass density ρ, velocity $\mathbf{v}$, energy per unit mass e, stress tensor σ and heat flux vector $\mathbf{Q}$.

$$\begin{aligned} d\rho/dt &= -\rho\nabla\cdot\mathbf{v} \\ \rho d\mathbf{v}/dt &= \nabla\cdot\boldsymbol{\sigma} \\ \rho de/dt &= \boldsymbol{\sigma} : \nabla\mathbf{v} - \nabla\cdot\mathbf{Q} \end{aligned} \tag{3}$$

As seen by the system Equations (1) to (3), the two models, MD and SPH, differ significantly. A transition between the models is attempted by using the MD equation for acceleration ($F = m\ddot{x}$), into the SPH Equation for particle acceleration (4). Crucial assumptions for this simplification are: the existence of no macroscopic density fluctuations in the fluid and a constant pressure $\mathbf{P}$ for the system [3]. If these conditions are met, then Equation (4), which

describes the acceleration in the SPH model, can be reduced to Equation (5). Where B is a constant, m is the mass of the unit particle, taken to be equal to one for simplicity and w_{ij}, the kernel function is equivalent to the pair potential ϕ_{ij}.

$$\ddot{\mathbf{r}}_{\mathbf{SPH}} \equiv -\sum_{i=1}^{N}\sum_{i<j} m[(\mathbf{P}/\rho^2)_i + (\mathbf{P}/\rho^2)_j] \cdot \nabla_i w_{ij} \tag{4}$$

$$\ddot{\mathbf{r}}_{\mathbf{SPH\ reduced}} = -\sum_{i=1}^{N}\sum_{i<j} mB \cdot \nabla_i w_{ij} \tag{5}$$

B. Basic System Properties

The fluid systems analysed in this report iterated through time using a standard Verlet algorithm, given from Equation (6). The Verlet algorithm utilised the values provided by the equation of forces (see Equation (2)) along with the velocities and positions of the particles to step though each iteration [1] and hence allow the system to develop over time.

$$\begin{aligned} \mathbf{v}_{t+\delta t} &= \mathbf{v}_t S + \mathbf{a}_t\ \delta t \\ \mathbf{r}_{t+\delta t} &= \mathbf{r}_t + \mathbf{v}_{t+\delta t}\ \delta t \end{aligned} \tag{6}$$

Furthermore, to eliminate the surface effect in the simulations, periodic boundary conditions were used. The simple cubic lattice was periodically repeated through space around the simulated cell [6]. Hence, when a particle went out of bounds from the unit cell, depending on the face of the unit cell that it passed through, an image of that particle would be mirrored inside the cell from the opposite face. The molecules were mirrored back to the unit cell by Equation (7), where r_i is the position of the particle relative to the origin and L is the length of the cubic unit cell in the *x-y-z* directions, given by the following relation: $L = (N/\rho)^{\frac{1}{3}}$. With ρ being the macroscopic density and N the number of particles simulated.

$$\begin{aligned} \mathbf{r}_i > L \quad &\text{then:} \quad \mathbf{r}_i = \mathbf{r}_i - L \\ \mathbf{r}_i < 0 \quad &\text{then:} \quad \mathbf{r}_i = \mathbf{r}_i + L \end{aligned} \tag{7}$$

To reduce calculation time for the simulation, a cut-off radius r_c was implemented that allowed the program to compare only particles that laid within the radius r_c. By default the

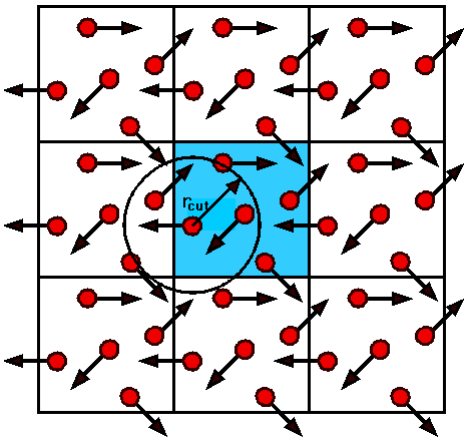

Figure 1: Demonstration of periodic boundary conditions [7].

cut-off radius was chosen to be half the length of the simulated unit cell, providing a significant computational boost, while at the same time ignoring insignificant contributions from distant particles that would have no effect in the final results.

C. Method

In this section the structure of the system will be discussed and a brief description of the code written will be given. The code itself was written purely in C++ and was optimised using an Intel compiler. In Figure 2, a flowchart is depicted, demonstrating the basic methods of the simulation. At first, the system needed to be initialised and most importantly conserve the momentum of the unit cell in order to avoid hydrodynamic flow. The velocities of the particles were scaled using Equation (8), where T is the temperature of the system, T_0 is the target temperature the system should operate and K_N, is the kinetic energy of N particles.

$$\begin{aligned} scale &= \sqrt{T_0/T} \\ T &= K_N/(3/2N) \end{aligned} \tag{8}$$

After initialisation, the separation distance between all the ij pairs in the fluid is calculated. Further on, the static properties of the fluid are calculated such as energies and pressures along with the *g(r)* for RDF. Then the simulation uses the Verlet algorithm described in Equation (6) to iterate. At this stage the periodic boundary conditions are imposed, giving the closest image of the particles in the unit cell. Finally, additional statistical properties, such as the MSD and VAF, are calculated. This procedure, excluding the initialisation is repeated for N_{steps}. A full

version of the code can be found in the GitHub repository [8]

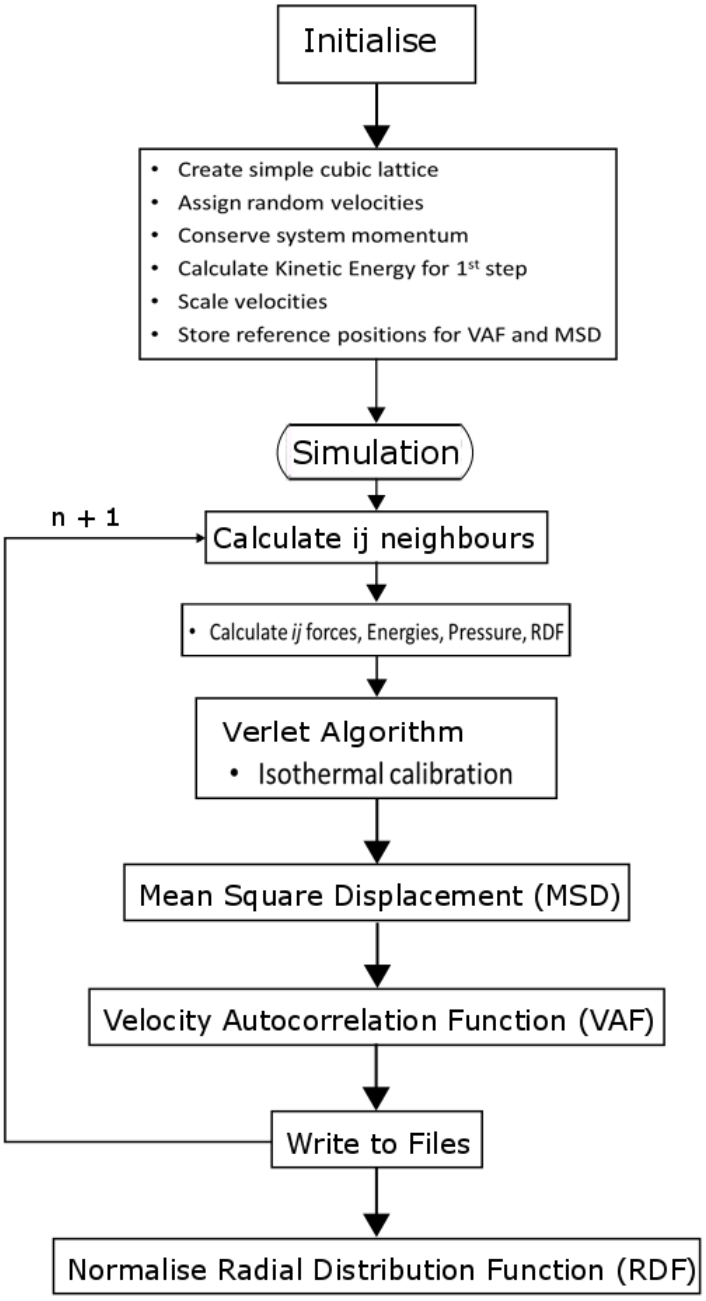

Figure 2: Flowchart of the MD simulation, demonstrating the main methods of the software.

III. SIMULATION RESULTS

Model dependence on parameter A and related parameters

The system simulations were focused around the sixth power n of the pair potential ϕ_{ij}, although additional data were obtained for a plethora of parameters n. In more detail, the core of the data collection process consisted of a number of particles $N = 512$, a density $\rho = 0.5$ and a number of steps $N_{steps} = 5000$ that the Verlet algorithm iterated through. For this set of initial conditions, simulations were run with the following values of n (5, 6, 7, 8, 9, 10, 12), where for each n fifteen values for A were taken (0.0, 0.25, 0.50, 0.75, 1.0, 1.25, 1.50, 1.75, 2.0, 2.25, 2.50, 2.75, 3.0, 3.50, 4.0).

Theory suggests that for all values of n, the pair potential has a singularity at the origin when $A = 0$ and it tends to 0 as either A or r tend to infinity. Physically, this behaviour can be described as "softening" of the pair potential. More analytically, A affects the pair potential in a threefold manner: For values of A smaller than 1, an increase in the potential strength n results into a stronger pair potential overall. When A is larger than 1, then an increase in n, delivers a weaker pair potential and for A equal to 1, the strength of the potential remains constant with only the gradient of the potential increasing. These characteristics of the potential, can be observed in Figure 3. By increasing A, the singularity at the origin of the potential is effectively removed at the expense of the maximum potential being decreased. Furthermore, the particle force f_i has a global maximum, at $\mathbf{r} = \pm\sqrt{A/(1+n)}$. The maximum in the force creates a "force-barrier" for the particles, which is translated to the pair potential as its point of inflection. Particles with kinetic energy less than that of the energy at the inflection point will experience strong repulsive forces. As the pair potential becomes "smoother" the energy required to pass the point of inflection decreases, resulting into particles being trapped in weak repulsive force regions, forming clusters.

The following subsections will be discussing the results for the radial distribution function (RDF), velocity autocorrelation function (VAF) and mean square displacement (MSD), in an attempt to interrupt the changes the fluid undergoes when system parameters are altered.

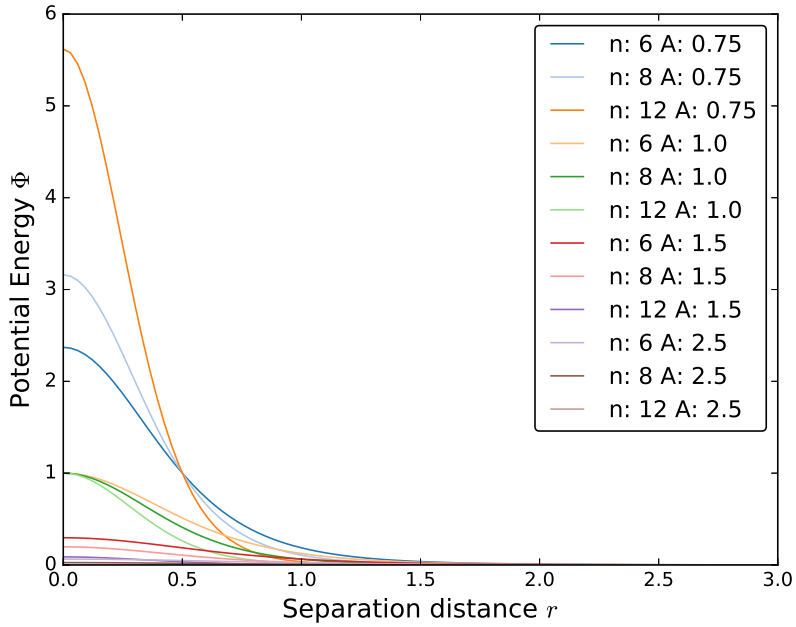

Figure 3: Dependency of the pair potential from Equation (1), for different n and A parameters.

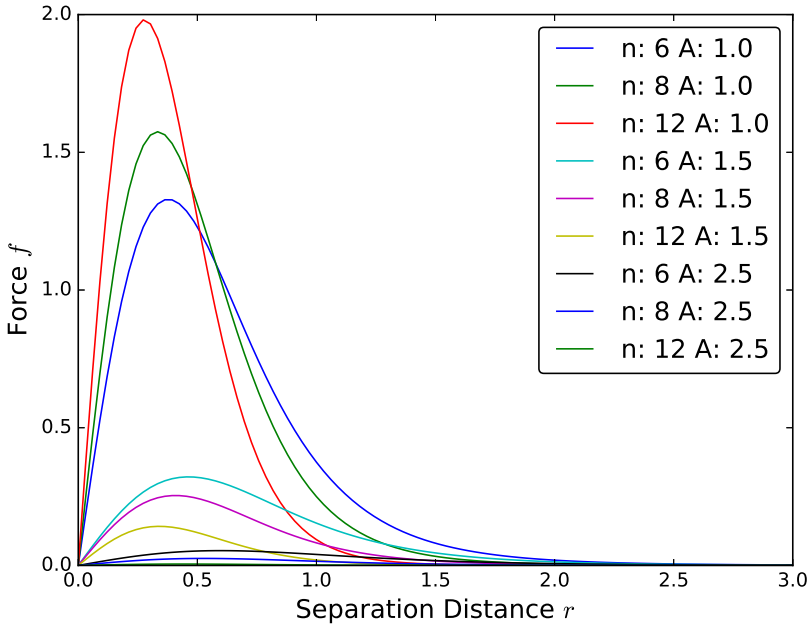

Figure 4: Multiple force functions based on Equation (2). A decrease in the maximum force is accompanied by a shift in the position of the maximum for increasing n and A.

A. Energies and Pressure

The average potential, average kinetic and total energy, per particle of the system provide important information about the state of the fluid. The energies were calculated using Equations Equations (9) to (11), respectively. With N being the number of particles in the fluid.

$$\Phi = \frac{1}{N}\sum_{i=1}^{N}\sum_{i<j}\frac{1}{\left(r_{ij}^2 + A\right)^{n/2}} \tag{9}$$

$$K = \frac{1}{2N}\sum_{i=1}^{N}\mathbf{v}_i^2 \tag{10}$$

$$E_{TOT} = K + \Phi \tag{11}$$

Below, are depicted the variations in energy of an isothermal fluid of density $\rho = 0.5$ with 5000 time steps and 512 particles. As expected, in Figure 5, the energies per run had minimal fluctuations. Since the potential energy was constant, through out the runs, the average was calculated in order to obtain a better understanding of the fluid. For increasing values of A the potential Φ and hence the total energy, tend to decrease, with the potential per particle approaching 0 as its limit. When the potential energy is small, then the thermal interactions dominate the system, implying the fluid has entered a weakly-interacting regime. In more detail, Figure 6 depicts the average Φ for multiple values of A over increasing values of the potential strength n. In the figure it can be observed, that for small changes in A, when A is smaller than 0.75, there is a disproportional decrease in the potential energy. Implying that molecular level interactions dominate the fluid and therefore it is still within the MD regime. As A increases past the value of 1.25, the values for the kinetic energy K (see Figure 5) are disproportionately greater than the potential and small changes in A have negligible impact on Φ for the system, implying minimal interactions between the particles. Consequently, the system is in the weak-interacting regime. By assigning upper and lower boundaries for the MD and weakly interacting regimes, the values for parameter A, that allow a transition to SPH, can be determined. Therefore, for A, between the two regimes, (0.75 to 1.25), should correspond to transition to the SPH model.

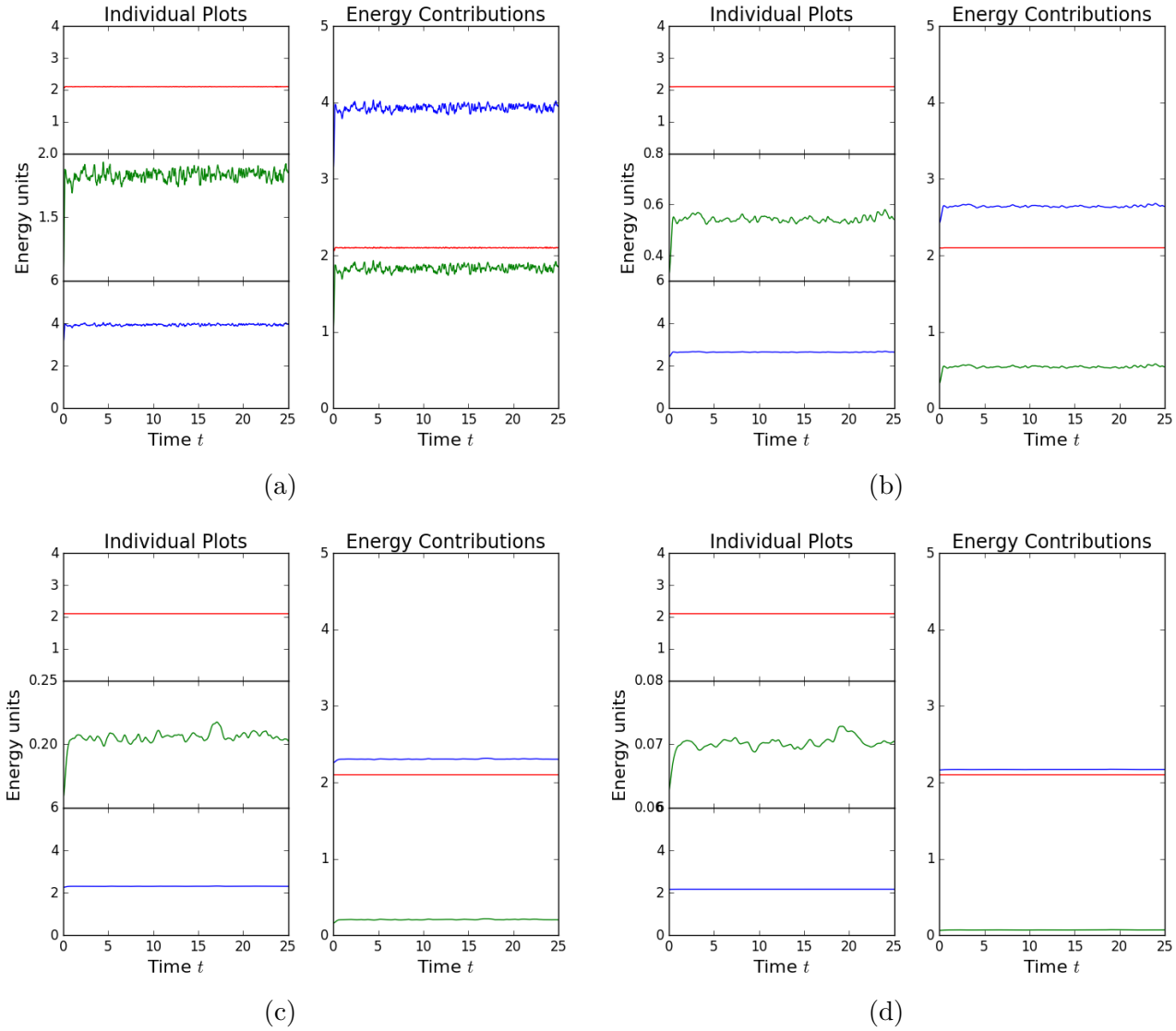

Figure 5: Energy diagrams of simulations for $n = 6$ with different A parameters. Average energies per particle for $N = 5000$ steps: (red) Kinetic energy K, (green) Potential Energy Φ, (blue) Total energy $(K + \Phi)$. (Plots on the right) Relative comparison of K, Φ, $K + \Phi$. The parameters of the different graphs are as follows: (a) A = 0; (b) A = 1; (c) A = 2; (d) A = 4. Systematic decrease of the potential energy, with an increase of A, while kinetic energy is conserved. At (c) and (d) the thermal effects appear to dominate.

In addition to the energy, the pressure of the system was also measured. The total pressure of the system is a combination of the pressure originating from the thermal properties of the fluid, which were kept constant, and the virial or configurational pressure P_C. Configurational pressure is defined by Equation (12) arising from a collective particle force, exerting a pressure

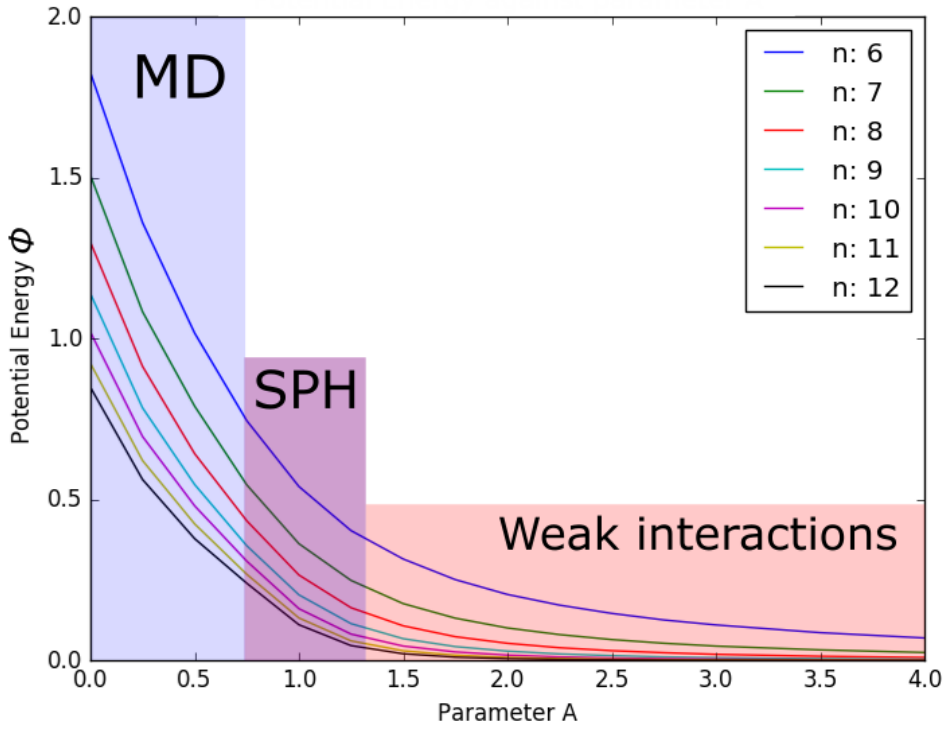

Figure 6: Decrease of Φ with increase of parameter A and n. A values close to 0 exhibit strong repulsive forces, in accordance with the MD regime. Large A values correspond to weak coupling of pairs, hence the fluid weakly interacts with itself.

to each particle individually.

$$P_C = \frac{1}{3V}\sum_{i=1}^{N}\sum_{i<j} r_{ij} f_{ij} = \frac{1}{3V}\sum_{i=1}^{N}\sum_{i<j} r_{ij}^2 n \frac{1}{(r_{ij}^2 + A)^{n/2-1}} \tag{12}$$

By performing basic statistical analysis of means and standard deviations on the collected data, it was determined that P_C is constant throughout the simulations, much like the energies. An example of the fluctuations that occur in P_C are Figures 7a and 7b and a complete table with the means is provided in Table 1. Due to the constant nature of P_C, the averages over time for the different pressures were allowed to be taken, the result is depicted in Figure 8.

Figure 8 provides consistent results as to the existence of the two extreme regimes, MD and weak-interactions region. The hypothesised SPH region, is more pronounced in the figure, backing with additional data, the existence of a transition between MD and SPH. Again, the hypothesised SPH regime is bounded between the A values of 0.75 and 1.25. In the next subsection the RDF will be discussed with respect to the three observed regimes.

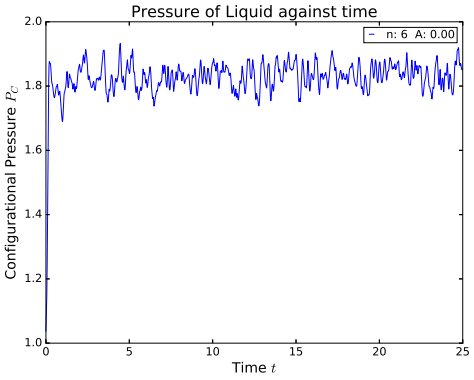

(a)

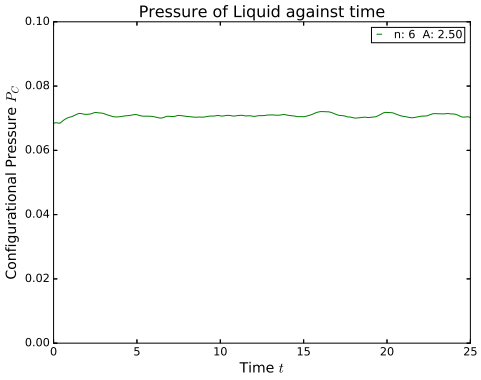

(b)

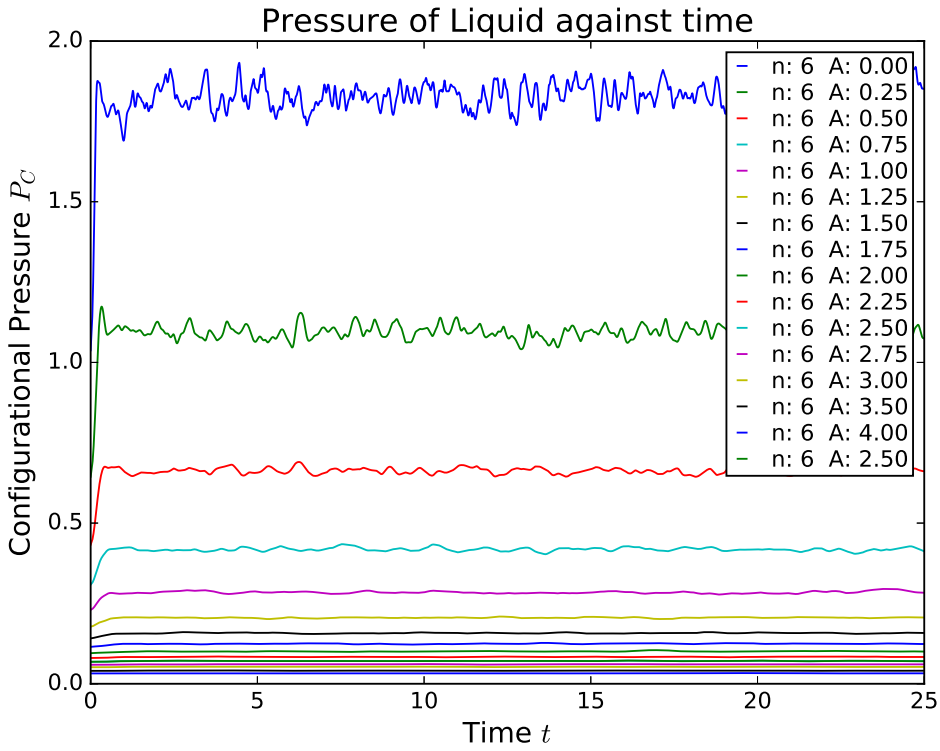

(c)

Figure 7: Configurational pressure plots: (a) $n = 6$, parameter $A = 0$; (b) $n = 6$, parameter A $= 2.5$; (c) P_C for different values of A at $n = 6$; Constant nature of PC for all tested values of A and n.

Table 1: Mean and standard deviation of the configurational pressure P_C over the time for $n = 6$. Demonstrates the constant nature of the configurational pressure for each run.

A	$\langle P_C \rangle$	stdev
0.00	1.83	0.06
0.25	1.09	0.04
0.50	0.66	0.02
0.75	0.42	0.01
1.00	0.284	0.006
1.25	0.205	0.003
1.50	0.157	0.002
1.75	0.124	0.001
2.00	0.101	0.001
2.25	0.0836	0.0008
2.50	0.0708	0.0006
2.75	0.0605	0.0004
3.00	0.0526	0.0004
3.50	0.0407	0.0003
4.00	0.0325	0.0002

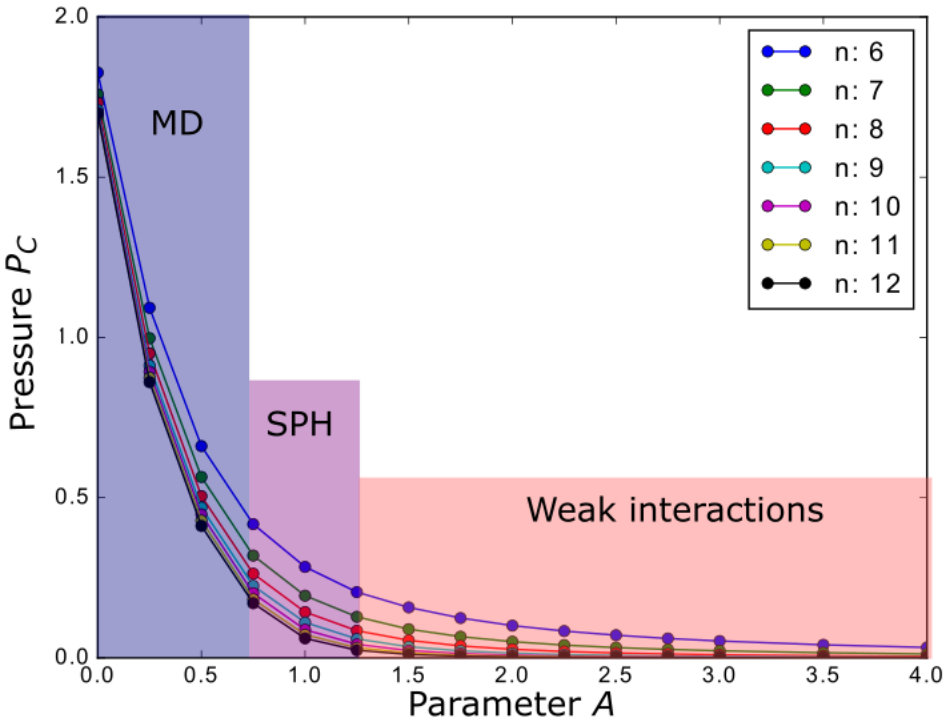

Figure 8: Average configurational pressure P_C for the standard range of values for A over increasing potential strength n. Exhibiting division fo regimes: lower values of A correspond to MD regime. Large A belong to weak-interactions regime. Hence values in between correspond to SPH.

B. Radial Distribution

The radial distribution function, RDF, is a measure of the particle-packing of the fluid, providing a value for the spherical density fluctuations that exist microscopically within it. All the systems examined were isotropic and hence there is no dependency on the orientation of the particles. The definition of *g(r)*, Equation (13), implies a proportionality between $\rho g(r) d\mathbf{r}$ and the probability of a particle being located in a volume element $d\boldsymbol{r}$ at a distance r from a reference particle. By considering a spatially homogeneous system, the integral is simplified to Equation (14), since only the relative separation distance between the particles is important[1].

$$g(\mathbf{r_1}, \mathbf{r_2}) = \frac{N(N-1) \int e^{\Phi(\mathbf{r_1}, \ldots \mathbf{r_N})/T} d\mathbf{r_3} \ldots \mathbf{r_N}}{\rho^2 \int e^{\Phi(\mathbf{r_1}, \ldots \mathbf{r_N})/T} d\mathbf{r_1} \ldots \mathbf{r_N}} \tag{13}$$

$$g(\mathbf{r}) = \frac{2V}{N^2} \langle \sum_{i<j} \delta(\mathbf{r} - \mathbf{r}_{\mathrm{ij}}) \rangle \tag{14}$$

To measure RDF, a histogram can be used containing n discrete values for the separation distance r. Then the descretized *g(r)* is given by 15. Where V is the volume of the system of N particles, in a shell of thickness Δr, containing h_n particles in that shell, with $r_n = (n - \frac{1}{2})\Delta r$[1].

$$g(r_n) = \frac{V h_n}{2\pi N^2 r_n^2 \Delta r} \tag{15}$$

For a system modelled with parameter $A = 0$ and $n = 6$ the results obtained for *RDF* were consistent with the hard sphere model using a Lennard-Jones potential. The particles in the fluid exhibit periodic clustering behaviour with their nearest neighbours and their next-nearest neighbours. Although clustering was present in the system the radius of the clusters was large, as seen from the r value corresponding to the peak in Figure 9a, resulting into a fairly homogeneous, in density, fluid. For $A = 0$ the repulsive forces of the potential are considerably strong and since *g(r)* is proportional to the probability of a particle being found a distance r from the reference particle, when *g(r)* is zero as seen in Figure 10a then the probability of two particles having a separation distance $r = 0$, is zero.

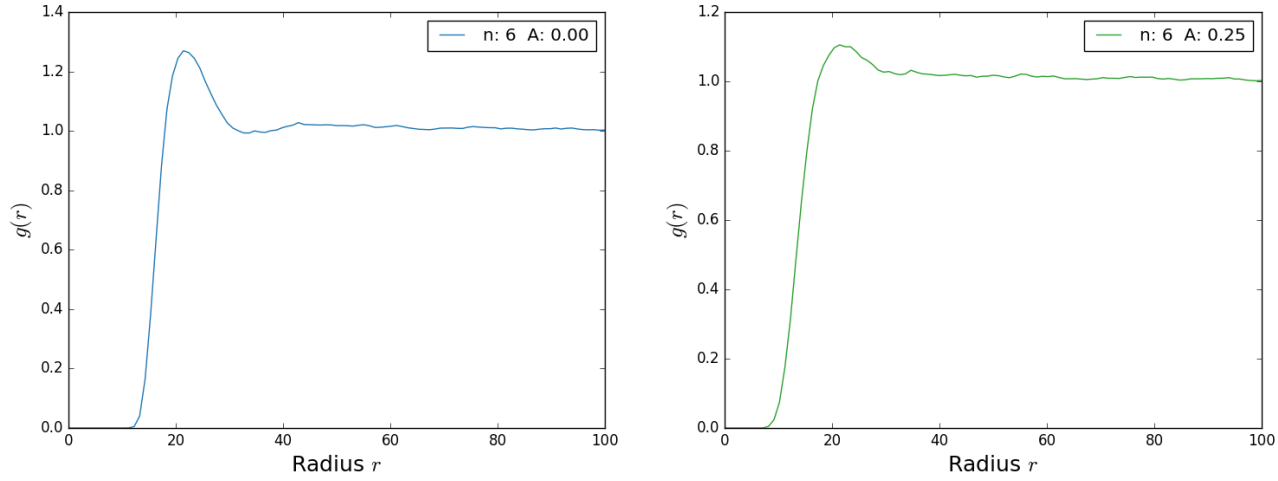

(a)

(b)

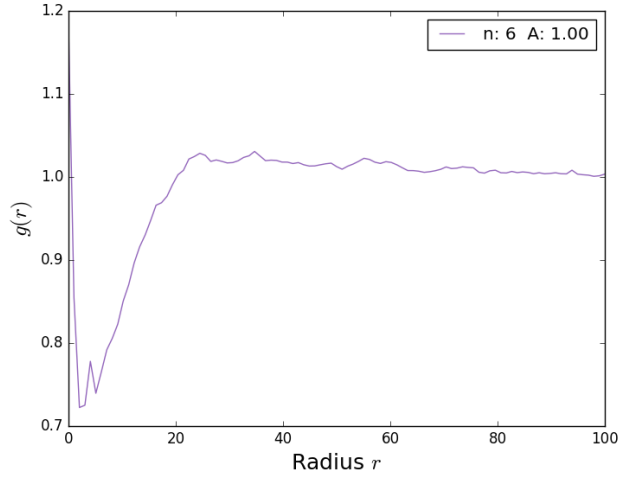

(c)

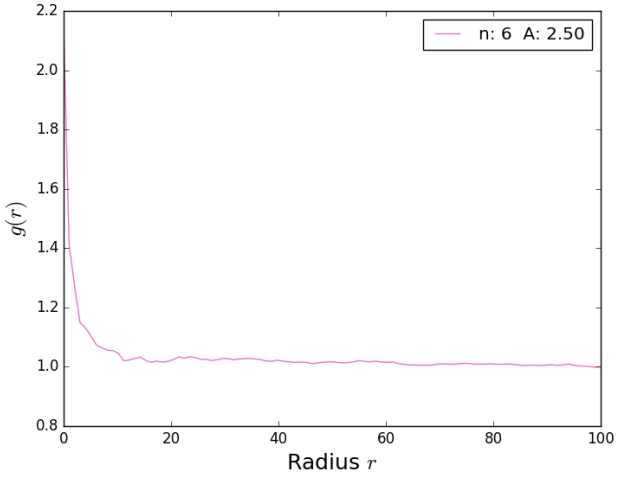

(d)

Figure 9: Radial Distribution Function plots for a fluid with $\rho = 0.5$ and $N = 512$ particles: *RDF* of pair potential $n = 6$; (a) RDF for $A = 0$; (b) RDF for $A = 0.25$; (c) RDF for $A = 1.00$; (d) RDF for $A = 2.50$. Gradual shift of the *g(r)* peak towards $r = 0$ with increasing A.

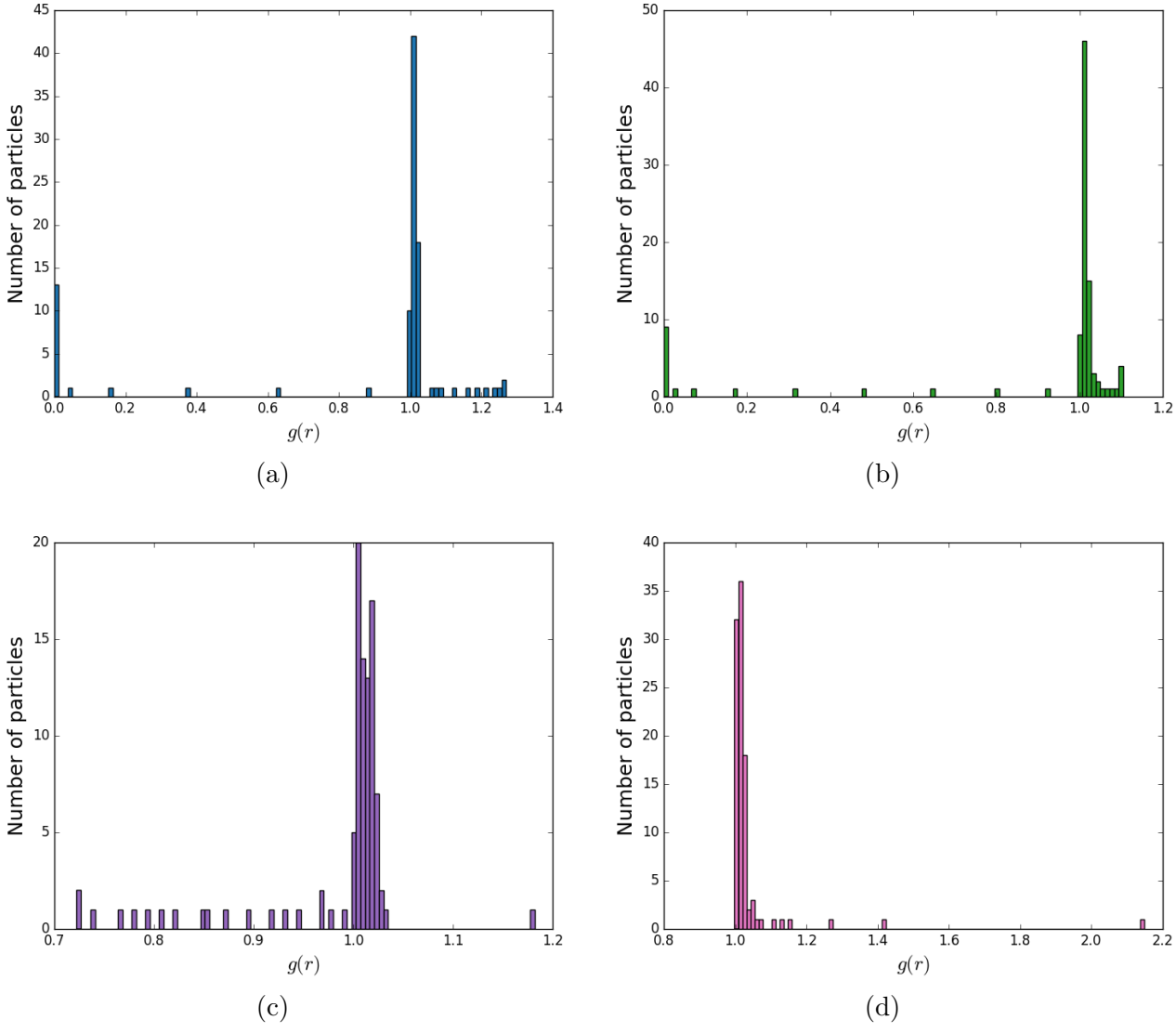

Figure 10: Histograms of *RDF*, with 100 bins, for a fluid with $\rho = 0.5$ and $N = 512$ particles. (a) $n = 0$; (b) $n = 0.25$; (c) $n = 1.00$; (d) $n = 2.50$. *g(r)* $\propto$ to the probability of finding a particle a distance r from the reference particle. Macroscopically, all the systems have *g(r)* = 1, implying no density fluctuations.

As the value of A increased from 0 to 0.5, while keeping n constant, a gradual decay was observed of the hard sphere characteristics for the system, in the RDF. The height of the peaks decreased, eventually reaching the value of 1, the limiting value for the system's saturation, see Figure 11a. Further increase of A resulted into a significant decline in the strength of the pair potential allowing particles to coexist in the same coordinates as seen in Figures 9c and 10c. For values of A between 0.5 and 1.0, the fluid exhibits a decrease in density for small radii and a systematic increase of clustering with separation distance 0. When A becomes greater than 1, the influence of the kinetic energy on the system is significantly greater than the pair potential interactions. Although the pair potential interactions are weak, Figure 9d suggests that for $r = 0$, denser and denser clusters of particles will be formed in the fluid as A increases. Interestingly enough, the initial peak in Figure 9d does not provide any information for the number of particles included in the clusters. The current interpretation of this phenomenon, is that a very small number of particles manage to have a minimal separation distance due to the weak coupling of the potential, thus creating micro clusters (2-3 particles), an attribute of the weak-interactions model.

It has to be mentioned, that the saturation value of *g(r)* always tends to 1 independently of the modifications in the pair potential, suggesting the density fluctuations will never influence the system macroscopically and that the system approaches an almost ballistic model, with no long range order as r increases [9].

An interesting phenomenon was observed while examining the *RDF* fluctuations over different strengths of pair potentials n. Isosbestic points were found in the systems that had small values of A. For A equal to 0 and 0.25 two isosbestic points were spotted, one before and one after the peak of the *RDF* (see Figures 12a, 12b). As the value of A increased the second isosbestic point quickly converged to the macroscopic limit of *g(r)* and hence can not be observed (see Figure 12d). The first isosbestic point exhibited a steady decrease when A increased but for A larger than 0.75 the point vanished, implying the existence of a correlation between, the isosbestic points phenomenon and the pair potential ϕ_{ij}.

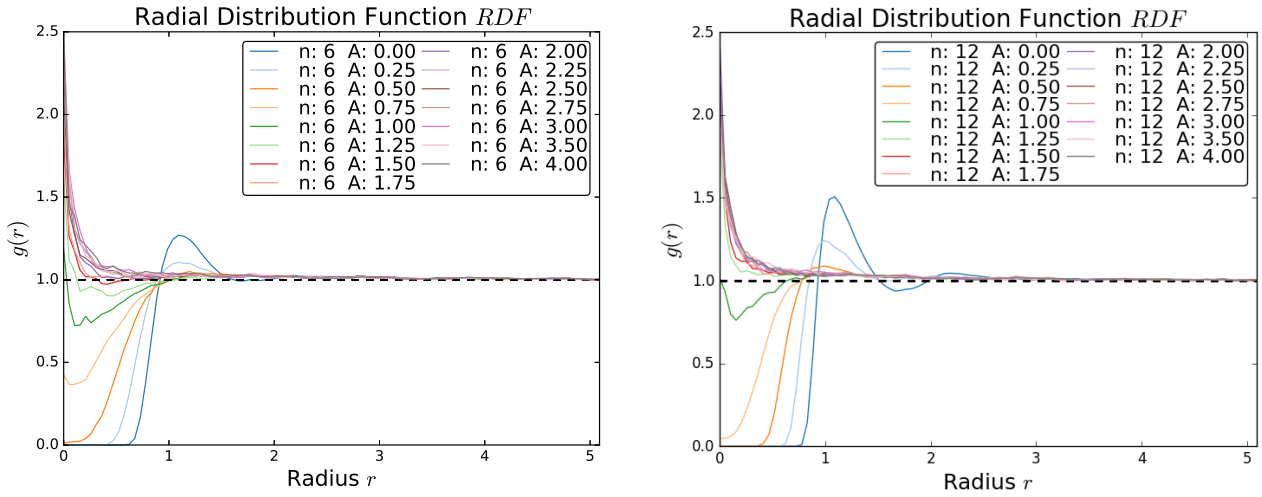

(a) (b)

Figure 11: Multiple RDFs (a) for $n = 6$; (b) $n = 12$. Transition from strongly repulsive to weak coupling pair potentials.

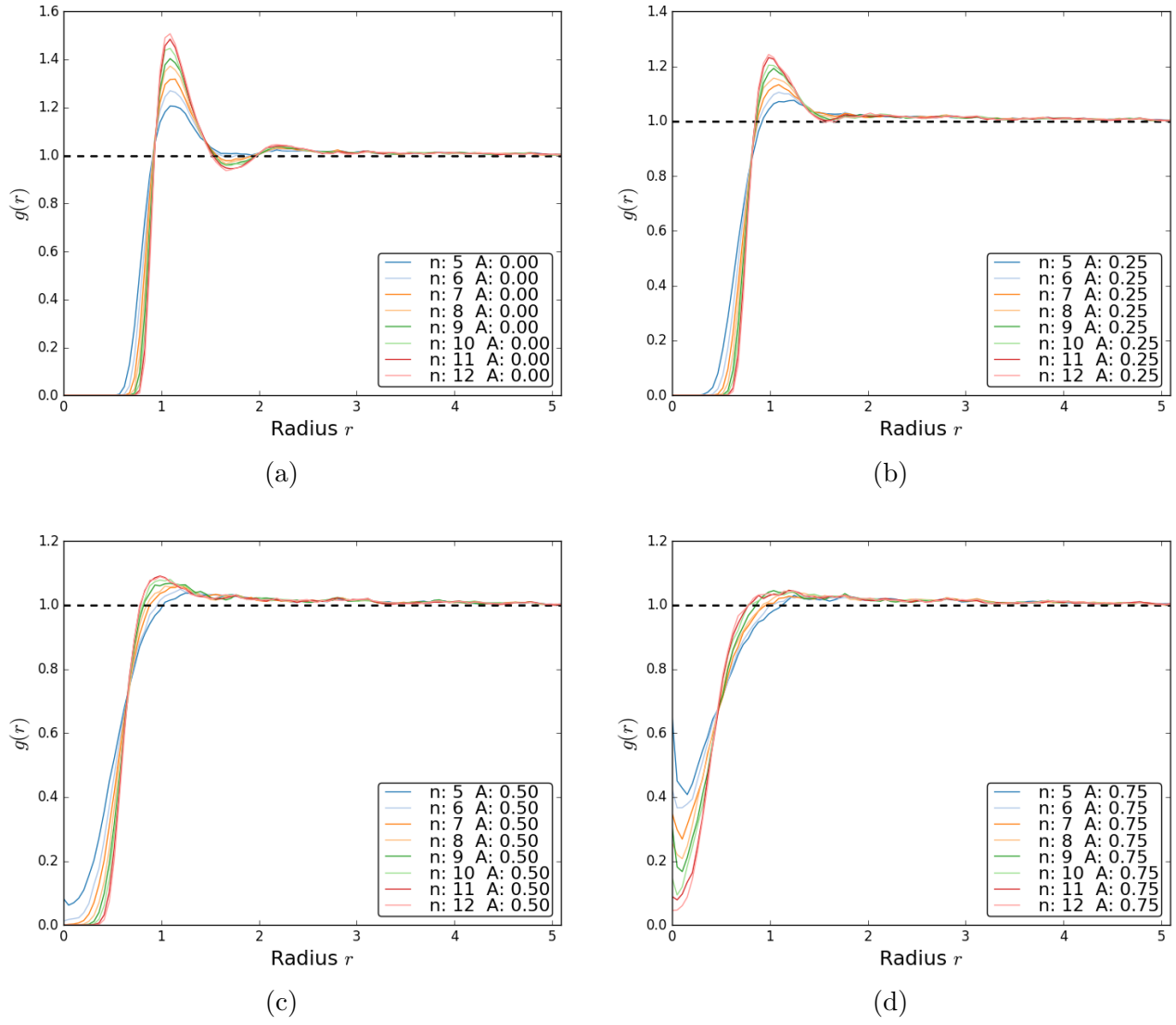

Figure 12: RDF plots for n = 5-12 with a constant value of A. Isosbestic points observed. Location of points depends on parameter A but only for the Lennard-Jones limit: (a) $A = 0$; (b) $A = 0.25$; (c) $A = 0.50$; (d) $A = 0.75$.

C. Velocity Autocorrelation Function

Velocity autocorrelation function (VAF) is a measure of the velocities' correlation from a reference time t_0 against the time development of the system. VAF is given by Equation (16), where $v_i(t_0)$ is the reference velocities at time t_0 [10].

$$C_v(t) = \langle \mathbf{v_i(t_0)} \cdot \mathbf{v_i(t}\rangle = \frac{1}{N}\sum_{i=1}^{N} \mathbf{v_i(t_0)} \cdot \mathbf{v_i(t)} \tag{16}$$

A perfectly correlated system, would be depicted in a VAF plot with a straight line parallel to the time axis. Since, the system has a "perfect" memory, the initial conditions of the particles are maintained. As a result, the difference of the initial velocity and time developed velocities of the particle will remain constant throughout time, hence resulting into a straight line plot [11]. On the contrary, a perfectly decorrelated system would be depicted by an abrupt change in the VAF near t_0, suggesting the loss of the system's initial conditions.

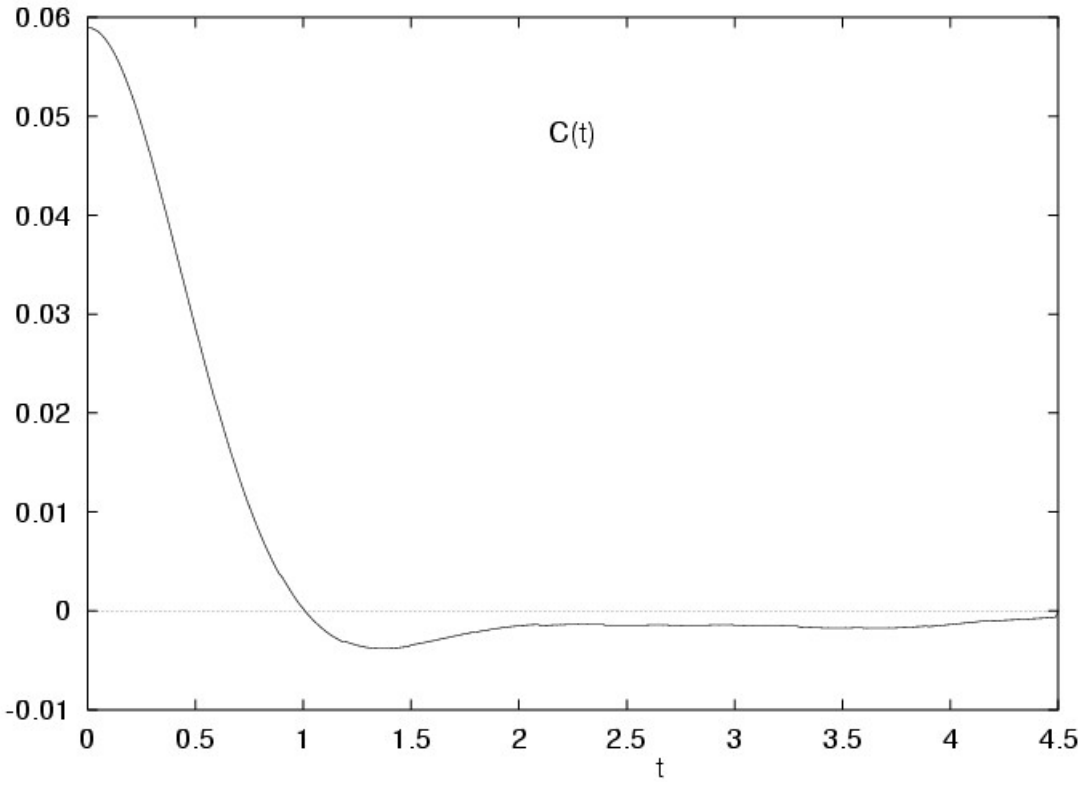

Figure 13: VAF plot for a Lennard-Jones model. Figure directly obtained from [12].

Theory suggests that the velocity decorrelation of a system in MD is described by two functions; the first containing an exponential decay factor describing the time interval when the decorrelation occurs and a secondary factor that linearises the VAF for large values of t [13]. For a MD model with particles being under the influence of a Lennard-Jones (LJ) potential, the expected VAF plot is given from 13. Since the system analysed in this paper resembles an only repulsive LJ system, the VAFs obtained from the various simulations should resemble the ones observed in Figure 13, with the only difference being the absence of the global minimum. The global minimum is a direct result from the particles balancing in a region between the attractive and repulsive forces of the LJ potential. The expected behaviour, was indeed observed for the simulated systems within the MD regime, as seen from Figure 14a.

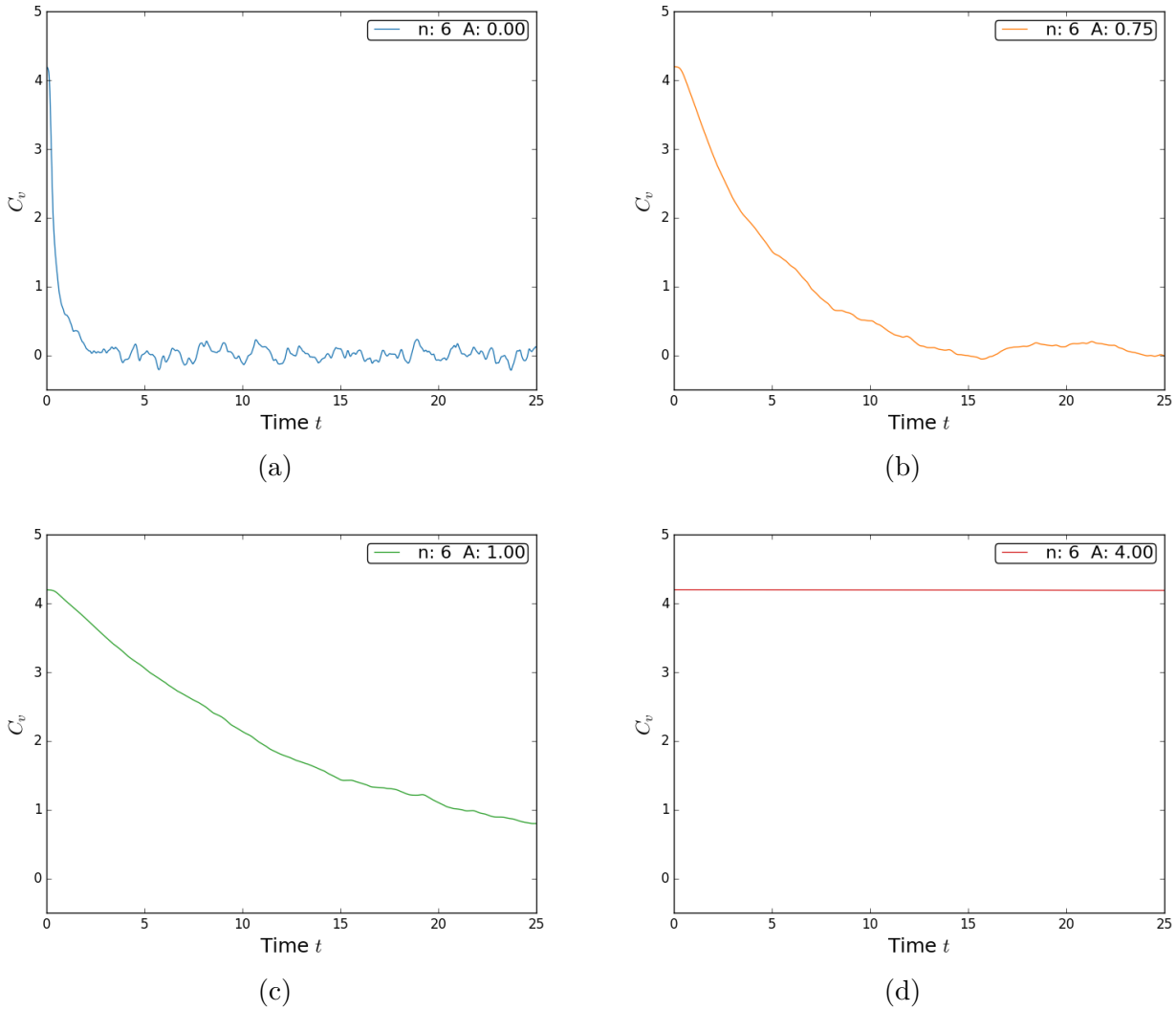

Figure 14: VAFs obtained using Equation (16) for $n = 6$, $N_{steps} = 5000$ and $\delta t = 0.005$: (a) $A = 0.00$; (b) $A = 0.75$; (c) $A = 1.00$; (d) $A = 4.00$.

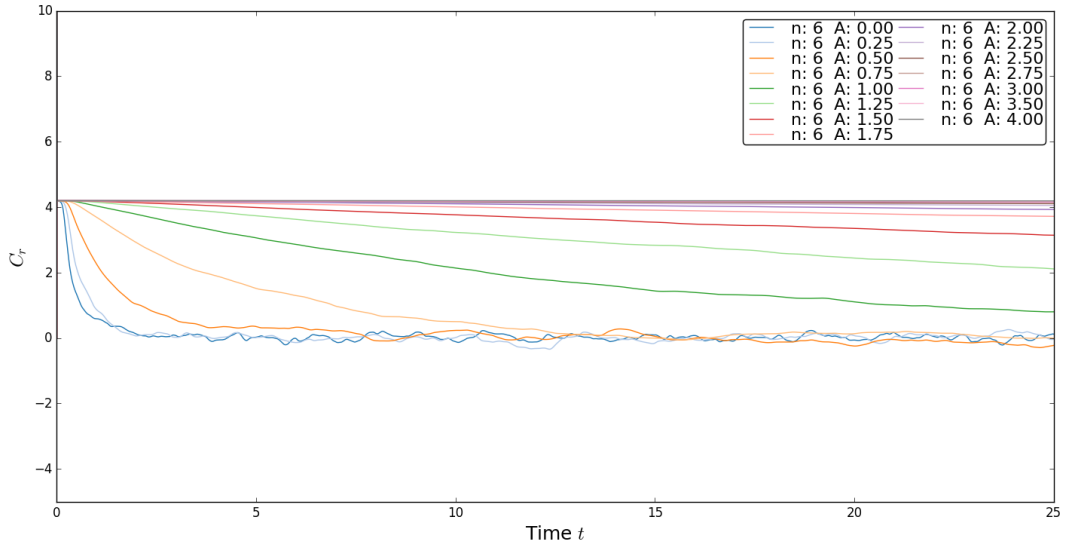

Figure 15: Correlation function of velocities for the average fluid particle with time development of 5000 steps.

Additionally, for the MD regime systems (small A), a rapid decorrelation of the velocities was observed near $t = t_0$. The system would maintain the decorrelated state for the rest of the simulation while exhibiting noticeable fluctuations in the VAF over time. The VAF fluctuations in Figure 14a are due to the noise of the system, which arises from the microscopic nature of the MD regime. The gradual increase of A, prolongs the time the system needs to decorrelate but eventually the fluid will cease to be correlated and will decay exponentially to 0, as seen in Figure 17, where VAFs from simulations of different number of steps are depicted. In Figures 15 and 16 VAF curves with A in the range of 0.75 to 1.00, demonstrate a "soft" decorrelation over time implying that there is a gradual loss of the systems' initial conditions. The "smooth" decay of the VAF is more visible in Figure 16, where systems with $A = 0.75$, exhibit a unique rate of decay for the VAF. This behaviour is consistent with the SPH model where system properties are uniformly distributed over the fluid. For A larger than 1.00 the system enters the weak-interactions regime were minimal decorrelation exists due to the weak coupling of the particles.

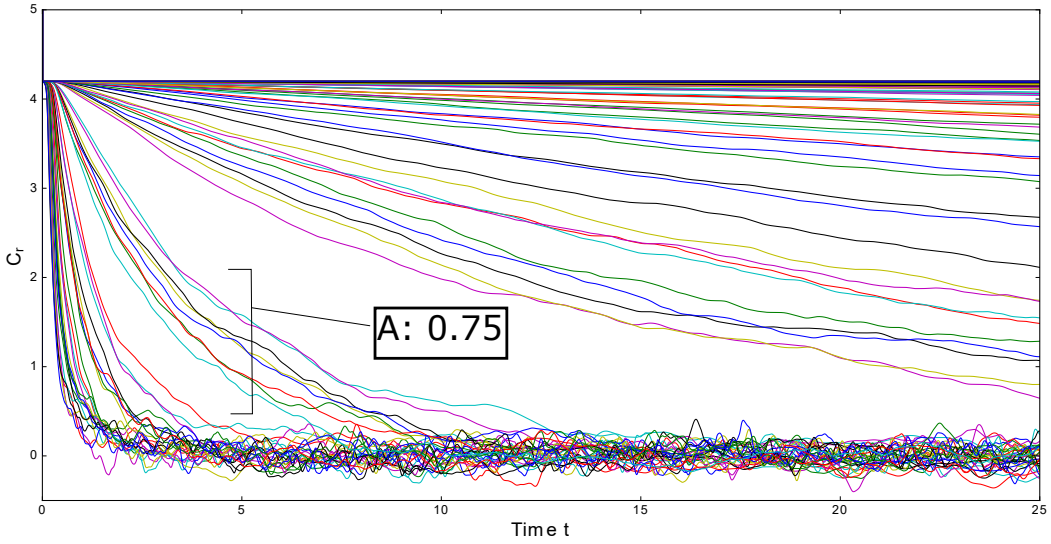

Figure 16: VAF for all integer values of n = 5-12 plotted against all values of A, for a system of $N_{steps} = 5000$ and $\delta t = 0.005$.

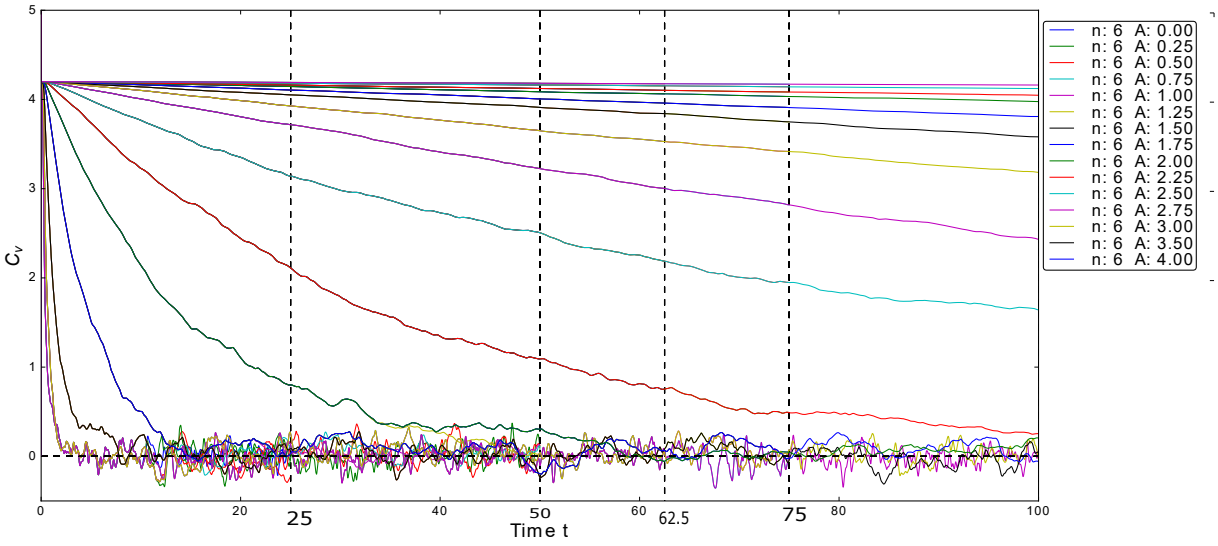

Figure 17: VAF for $n = 6$ and various A over different durations of simulated systems. Vertical dashed lines represent different durations for simulations ranging from 25 to 100 time units.

D. Mean Square Displacement

The mean square displacement (MSD), is a measure of the displacement of the particles from a position at a reference time t_0. The reference time, was chosen to be at $t_0 = 0$, when the particles were in the simple cubic lattice formation. The square of the displacement is then calculated for each particle as time t advances. The standard time of 5000 time steps was used to obtain the following data in Figure 18. MSD is given by the first equality of Equation (17) and for a three dimensional fluid, that diffuses in time the diffusion coefficient D can be extracted from the slope of MSD, see second equality of Equation (17)

$$MSD(t) = \langle (r_i(t) - r_i(t_0))^2 \rangle = 6Dt + C \tag{17}$$

Where MSD is an average over all i particles of the fluid at time t and D and C are a constants for the diffusion rate and y-intercept, respectively. Ideally C should be zero, for systems that diffuse completely. Additionally, the value of 6 appears as a constant of proportionality reflecting the three dimensional nature of the system.

The four plots in Figure 18, from left to right, top to bottom, show a gradual increase of the slope and hence D as the parameter A increases, implying an increase in the rate of the systems' diffusion. Moreover, the the MSD plots show significant non-linear behaviour at the origin as the value of A increases. This is caused due to the softening of the pair potential which results into the system diffusing over longer periods of time or completely lacking a diffusion. The definition of MSD is based on the principal that the particles in a fluid will move randomly a distance λ until they collide with their nearest neighbours and then they will change orientation and they will repeat the process indefinitely. In this case, the particles are ideal, they do not have physical coordinates and hence they are allowed to coexist in the same space coordinates at the same time, without violating the laws of the system. Even though, collisions between particles cannot occur since the particles are dimensionless, the hard core repulsion that governs them is sufficient to cause the system to diffuse.

The reason why particles do not coexist at all times is due to the fact that hard core repulsion is present when A is close to zero. By increasing A, the repulsive forces between the particles become weaker, allowing some particles with the appropriate energy to pass through the "barrier", at the point of inflection, imposed by the pair force (see force Figure 4). These

particles, under the influence of a weak pair potential, that lack interactions with their neighbours are responsible for the shape of diffusion plots with large value of A, observed in Figures 18d and 19. The actual shape of the MSD for a system that is not diffusing is a quadratic. If there is no particle repulsion, then each particle will move with an approximately constant velocity, then the distance travelled by the particle will be proportional to time and therefore, the square of that distance will be proportional to the time squared [14].

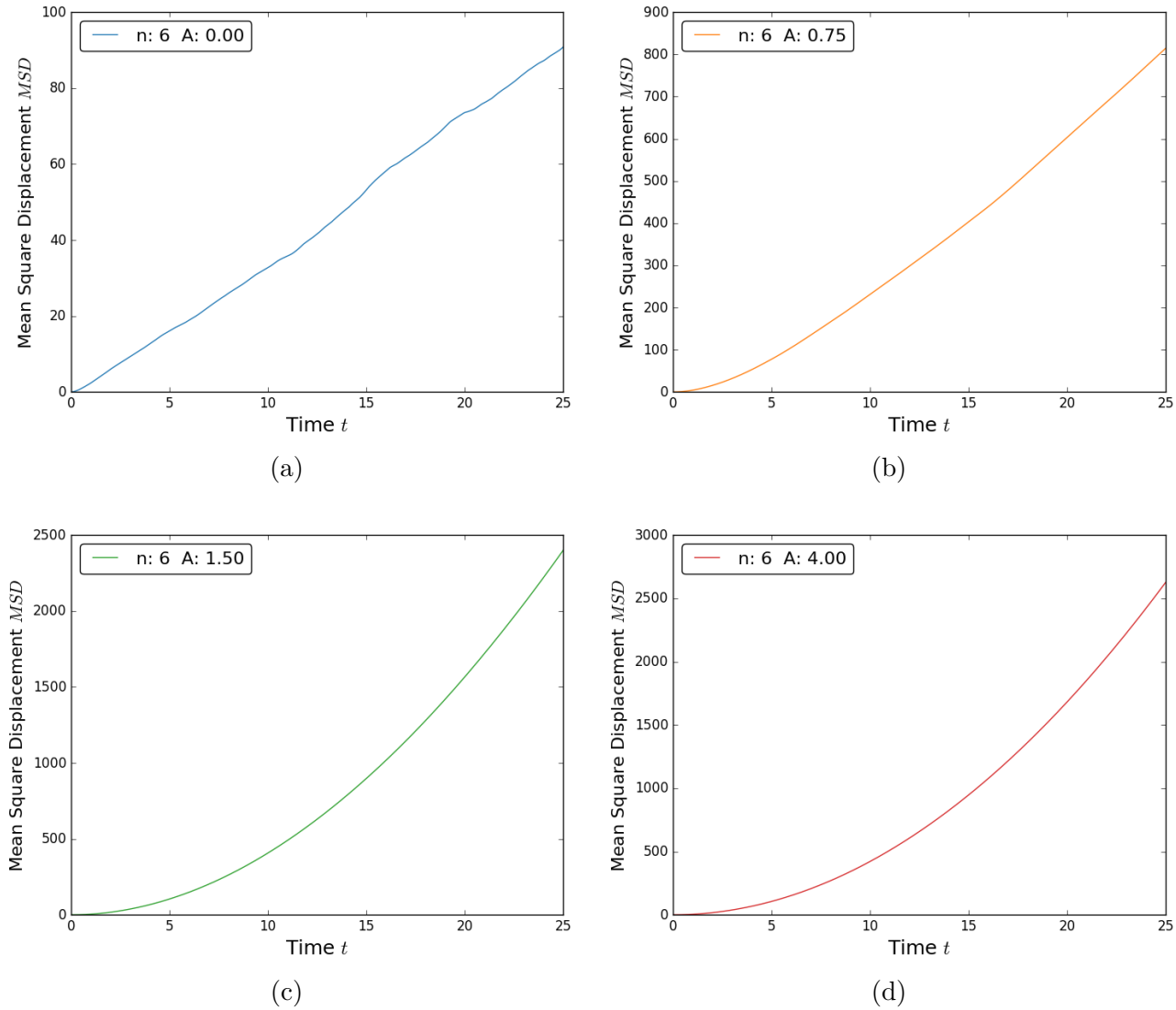

Figure 18: MSD plots obtained with Equation (17), for $n = 6$, $N = 512$ and $T_0 = 1.4$: (a) $A = 0$; (b) $A = 0.75$; (c) $A = 1.50$; (d) $A = 4.0$. For strongly repulsive potentials (a) the system diffuses quickly but for smoother potentials with weak coupling (d) the fluid never diffuses.

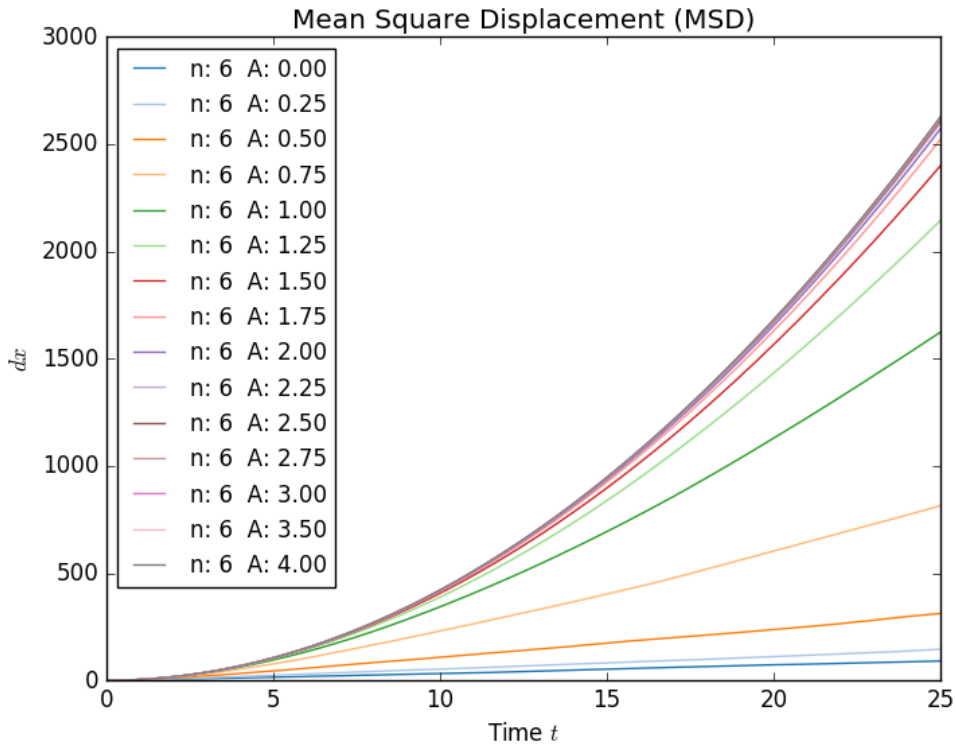

Figure 19: MSD for $n = 6$, $N = 512$ and $T_0 = 1.4$ for the standard range A. A systematic increase of the MSD values is observed implying an increase in the separation distance between the particles.

The MSD data from Figure 19 were fitted with a linear least-squares regression since the diffusion plots are theoretically proportional to time and the parameters of the fits are included in in Table 2. This process was repeated for all the potentials between 6 and 12, then diffusion coefficients D were plotted with respect to A, resulting into Figure 20a. From the Figure, it is apparent that the diffusion coefficient for a system of fixed time t reaches a saturation limit for large values of A, independently of the strength of the pair potential. The strength n of the potential only affects the rate at which a system attains the saturation limit, since systems with smaller values of n manage to diffuse for a wider range of A values.

Furthermore, the behaviour of how the value of the diffusion coefficient changes with different simulation lengths was investigated. Multiple simulations were run focused around the sixth power of the pair potential. A range of time steps was examined starting from 2500 up to 20000 but with the time increment being kept constant to $\delta t = 0.005$, the information was processed, extracting the linear least-squares regression parameters for each individual system. Afterwards, the saturation limit for D of each simulation was calculated and was placed in

Table 3, along with the duration of the simulation. The relationship for the increase of the diffusion coefficient with time becomes more comprehensible when the two quantities are plotted against each other. Figure 21 depicts that exact relation. As seen from the figure, the diffusion coefficient tends linearly to infinity as time increases. Theoretically, the slope of Figure 21 is the time derivative of the MSD equation, (see Equation (17)), and it is given by Equation (18). Where $\mathbf{v}$ and $\mathbf{r}$ refer to the square difference for the velocity and displacement accordingly, from a reference value. While the Boltzmann constant, $k_B = 1$ and the isothermal temperature of the system $T_0 = 1.4$. Hence, the theoretical result for the slope is equal to 4.20, while the experimental result obtained was 4.18 from the best fit line, providing a variance of only 2%.

$$
\begin{aligned}
&\mathbf{v} : constant \Rightarrow \mathbf{v} = \mathbf{r}/t \\
&MSD = \langle (\mathbf{v}t)^2 \rangle \\
&\qquad = \langle \mathbf{v}^2 \rangle t^2 \\
&\text{Energy equality:} \\
&\frac{1}{2} m \langle \mathbf{v}^2 \rangle = \frac{3}{2} k_B T_0 \\
&\langle \mathbf{v}^2 \rangle = 3 k_B T_0
\end{aligned}
\tag{18}
$$

Table 2: Data obtained by using a linear least-squares regression on the set of points in Figure 19. Fit parameters were calculated for the full range of A values, with $N_{steps} = 5000$ and a time step of $\delta t = 0.005$. Diffusion coefficient D along with the its corresponding fitting errors, while y_0 is the intercept of the fitter on the y-axis.

A	$6D$	y_0
0.00	3.75278 ± 0.0008	-3
0.25	5.813 ± 0.001	-4
0.50	12.814 ± 0.004	-17
0.75	34.11 ± 0.03	-86
1.00	67.4 ± 0.1	-236
1.25	87.6 ± 0.3	-341
1.50	96.9 ± 0.3	-391
1.75	101.3 ± 0.3	-416
2.00	103.1 ± 0.4	-426
2.25	104.0 ± 0.4	-431
2.50	104.4 ± 0.4	-433
2.75	104.7 ± 0.4	-435
3.00	104.8 ± 0.4	-436
3.50	105.0 ± 0.4	-437
4.00	105.1 ± 0.4	-437

Table 3: Maximum values of $6D$ coefficient for different simulation lengths.

Time t	$6D$	D error
12.5	52.59	0.3
25	105.1	0.4
50	209.8	0.5
62.5	262.17	0.6
75	314.5	0.7
100	419.0	0.8

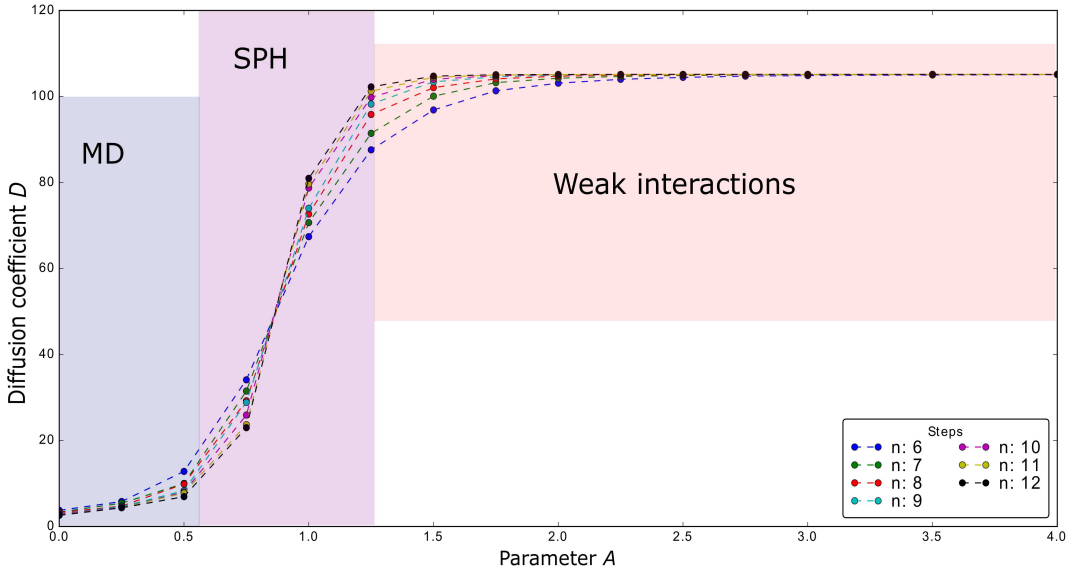

(a)

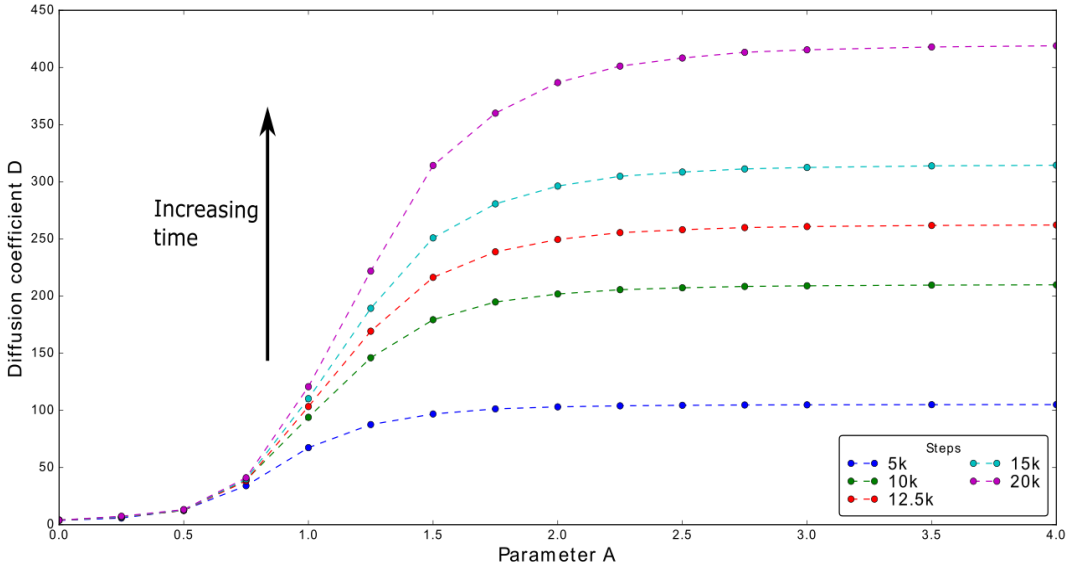

(b)

Figure 20: (b) Diffusion coefficient plot for $n = 6$ against A. Multiple simulation lengths are included to demonstrate the increasing saturation limit of D for undiffused systems as time increases.

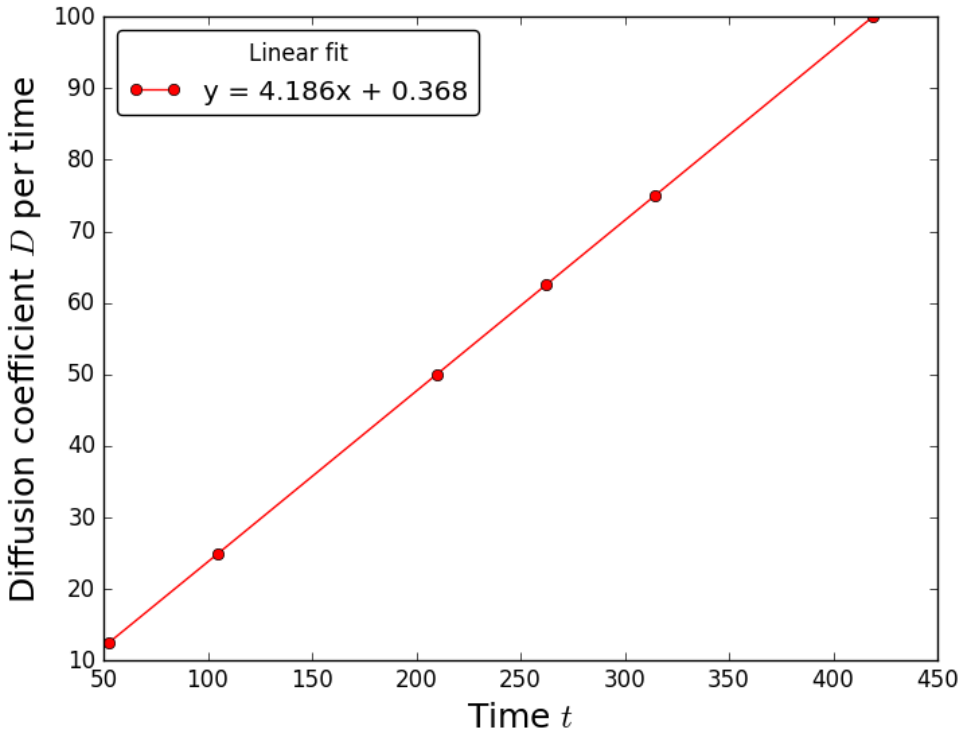

Figure 21: Increase of saturated D with time. D linearly tends to infinity implying no diffusion for large A. The slope of graph is equal to $3T_0$, where T_0 is 1.40.

E. Fluid Snapshots of Particles

The above Sections, A. - D., analysed in detail the data obtained from the simulated systems and attempted to support with evidence the objective of this report; that there exists a continuous transition between MD and SPH. In this section, an approach through visual inspection of the fluid will be followed in order to provide further evidence for the transition. It should be mentioned that results obtained through visual inspection have a significant uncertainty since they are dependent on the individual analysing the data.

At first, a simple system of $N = 512$ particles was analysed, inside an isothermal container at temperature $T_0 = 1.4$ temperature units, with a constant macroscopic density $\rho = 0.5$. The images in Figure 22, depict particles with their corresponding velocities in the form of vector arrows. The colour-bar on the left of the figures corresponds the position of the particles in the z-axis. When the fluid is in the MD regime, ($A \approx 0$), no short-range clustering is observed but since MD is a microscopic regime, short range density fluctuations are present (proven by the RDF in Figure 9a). As A increases to the critical limit for SPH, between 0.75 and 1.00, weak coupling between particles is present, then collectives of particles are observed near the same z-coordinates. The fluid at this stage has been coarse-grained and has effectively abandoned the microscopic MD regime and it has entered the mesoscopic regime of SPH. In Figure 23a, 2744 particles were used, providing a clear demonstration for the formation of clusters. The existence of the coarse-graining effect for some values of A, is a direct consequence of the inflection point that is present in the pair potential, as discussed in Section D.. For sufficiently large values of A, it has been deduced that the interactions between the particles are too weak, forcing them to move almost ballistically. This behaviour defines a new regime, named for the purpose of this report weak-interactions. For this regime it was theorised in Section B. that micro-clusters are formed, in an attempt to interpret the the near-zero peaks in the RDF of Figure 11. Micro-clusters are indeed observed in Figure 22d but in addition to that, large areas which were unoccupied by particles were detected. Further evidence to support this statement are provided in Figure 23b, where 2744 particles were simulated, and Appendix A.

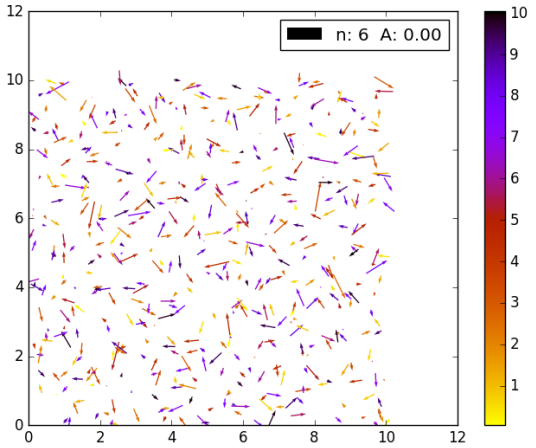

(a)

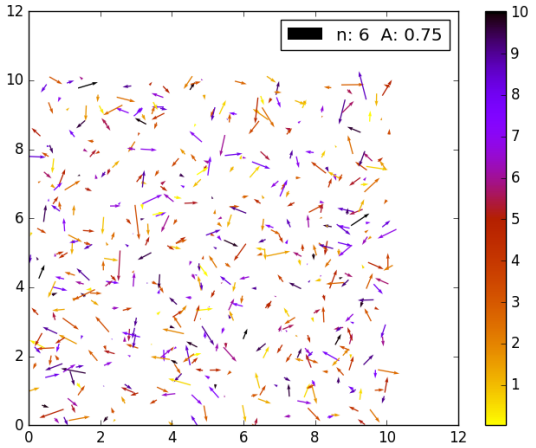

(b)

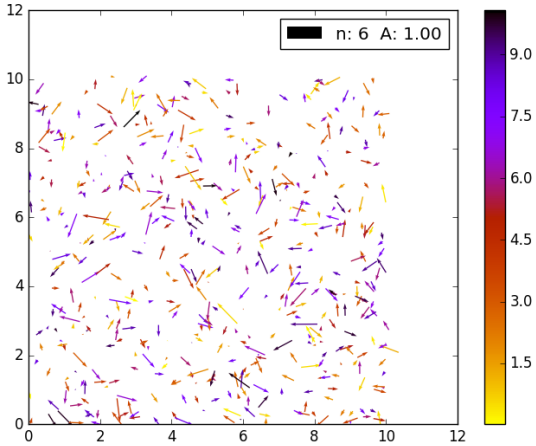

(c)

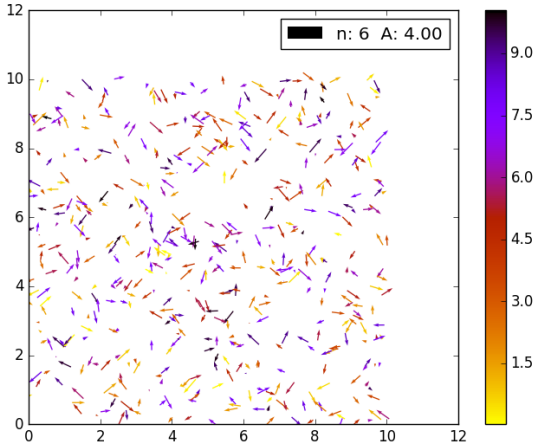

(d)

Figure 22: Snapshots for the fluid with $n = 6$ and different A parameters for the pair potential. (a) $A = 0$; (b) $A = 0.75$; (c) $A = 1.00$; (d) $A = 4.0$. The colour bar corresponds to the z-axis.

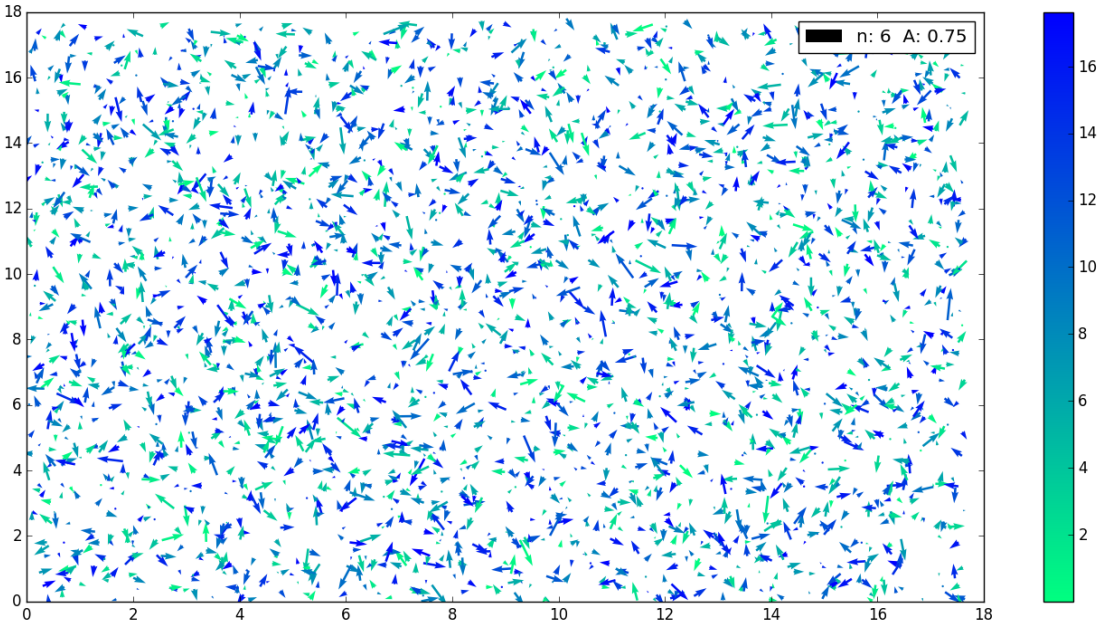

(a)

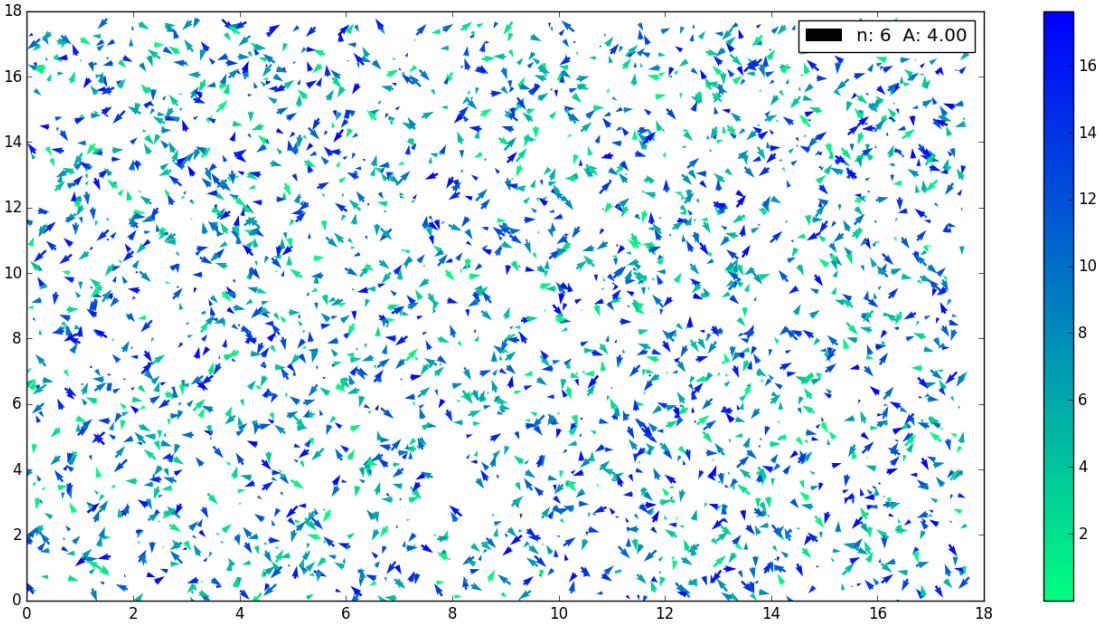

(b)

Figure 23: Number of particles $N = 2744$ in order to observe closer packing of the fluid. (a) n =6, $A = 0.75$; (b) $n = 6$, $A = 4.00$.

IV. CONCLUSIONS

In this report it was investigated if it is possible to transition continuously and isothermally from the microscopic MD regime to the mesoscopic SPH regime. In order to achieve this transition, simplifications had to be made to the SPH model, by keeping constant the system density ρ and pressure $\mathbf{P}$. The transition was partially achieved but in the process of doing so, a second mesoscopic regime for the fluid was discovered. Therefore, the fluid could transition between three regimes, when A was altered. As parameter A increased a coarse-graining effect was created, reducing the number of degrees of freedom for the particles and forcing them into clusters. The coarse-graining effect peaked for the SPH regime when A equalled 0.75-1.25. Further increase of A resulted into a transition to the weak-interactions regime.

All the processed data, returned a consistent result for parameter A, for the transient threshold between MD and SPH, with A being equal to 0.75 for the lower bound of the regime and 1.25 for the upper. The radial distribution function (RDF) provided crucial information about the structure of the fluid when A was altered. Due to data from the RDF, it was possible to theorise about the existence of micro-clusters in the weak-interactions regime, which were later observed in the flow snapshots of the fluid. Additionally, from the MSD and VAF it was found that, when the fluid was in the weak-interactions regime, the system would never achieve diffusion and would remain correlated, independently of the simulation's time length. A relation was found for the diffusion coefficients of the weak-interactions regime, where the rate of diffusion linearly tends to infinity over time, with a slope of $3T_0$.

Moreover, the transition to SPH was partially achieved because, in theory a fluid in the SPH regime should have minimal density fluctuations in its *g(r)*, when r is small. Although experimentally, it was observed that for As ascribed to the SPH regime, there were substantial fluctuations for the *g(r)* at small r. A result that most likely arises from the way the pair potential is defined. Even though the SPH transition was not perfect, the fluid exhibited significant signs of coarse-graining when the potential was smoothened and uniformity for its microscopic density.

Another finding of this report, were the isosbestic points in the RDF analysis obtained when A was kept constant and n was increased. These points did not have an easily traceable value but they shifted to smaller values in the x and y axis as the particles became smoother. At

this stage, the origin of the points is unknown, but the phenomenon is possibly related to the point of inflection in the pair potential.

To conclude, the main objective of this report was met, but due to time limitations the system was not analysed to its full extend. Additional research could be done by using multiple types of pair potentials and comparing them with standard SPH kernel functions such as Lucy and Monaghan, to observe similarities, if any, between a MD coarse-grained system and a purely SPH system. Also, an in-depth analysis for different target temperatures and macroscopic densities could be performed, in order to study the system's response. Attempts were made to analyse these systems but due to lack of time the results are incomplete and cannot be presented. Overall, the MD method with a coarse-graining parameter can function as a powerful analysis instrument for a SPH model, while having a fraction of the complexity SPH models have.

References

[1] D. C. Rapaport. *The Art of Molecular Dynamics Simulation:*. Cambridge University Press, Cambridge, 2 edition. doi:10.1017/CBO9780511816581.

[2] B. J. Alder and T. E. Wainwright. Studies in molecular dynamics. i. general method. *The Journal of Chemical Physics*, 31(2):459–466, 1959. doi:10.1063/1.1730376.

[3] Oyeon Kum, William G. Hoover, and Harald A. Posch. Viscous conducting flows with smooth-particle applied mechanics. *Phys. Rev. E*, 52:4899–4908, Nov 1995. doi:10.1103/PhysRevE.52.4899.

[4] Martin Pütz and Peter Nielaba. Insights from inside the spinodal: Bridging thermalization time scales with smoothed particle hydrodynamics. *Phys. Rev. E*, 94:022616, Aug 2016. doi:10.1103/PhysRevE.94.022616.

[5] Harald A. Posch, William G. Hoover, and Oyeon Kum. Steady-state shear flows via nonequilibrium molecular dynamics and smooth-particle applied mechanics. *Phys. Rev. E*, 52:1711–1720, Aug 1995. doi:10.1103/PhysRevE.52.1711.

[6] G. Makov and M. C. Payne. Periodic boundary conditions in ab initio calculations. *Phys. Rev. B*, 51, Feb 1995. doi:10.1103/PhysRevB.51.4014.

[7] Alex S. Ct Bill Smith Philip J. D. Lindan. Democritus periodic boundary conditions. URL: http://www.compsoc.man.ac.uk/~lucky/Democritus/Pictures/pbc-mi.gif.

[8] Ioannis Nikiteas. Md-simulation. URL: https://github.com/GiannisNikiteas/MD-simulation/tree/Isothermal.

[9] Professor A. Martini. Short course on molecular dynamics simulation.

[10] Leonid Zhigilei. Introduction to atomistic simulations. URL: http://www.people.virginia.edu/~lz2n/mse627/notes/Correlations.pdf.

[11] Philip J. D. Lindan Alex S. Ct, Bill Smith. The velocity autocorrelation function. URL: http://www.compsoc.man.ac.uk/~lucky/Democritus/Theory/vaf.html.

[12] Prof. Dr. Franz J. Vesely. Autocorrelation functions, Feb 2017. URL: https://homepage.univie.ac.at/franz.vesely/simsp/jsm/c4_evalu_s1_evalu.html.

[13] R.F.A. Dib, Fouzia Ould-Kaddour, and Dominique Levesque. Long time behaviour of the velocity autocorrelation function at low density and near critical point of simple fluids. *Physical Review E : Statistical, Nonlinear, and Soft Matter Physics*, 74, Jul 2006.

[14] Philip J. D. Lindan Alex S. Ct, Bill Smith. The mean square displacement. 2001. URL: http://www.compsoc.man.ac.uk/~lucky/Democritus/Theory/msd.html.

[1]Word count: 4972

1∗

A

Particle Plots

Systems were simulated for multiple combinations of parameters. More specifically, data were obtained for fluids that consisted of more particles or with higher densities. In this appendix some of this systems will be displayed, further proving the coarse-graining effect, softening the potential has on the fluid.

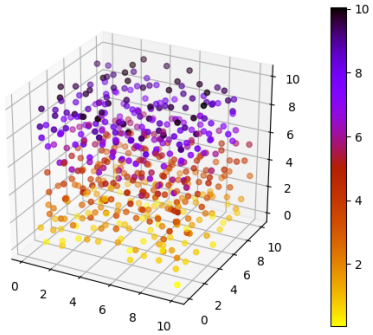

(a)

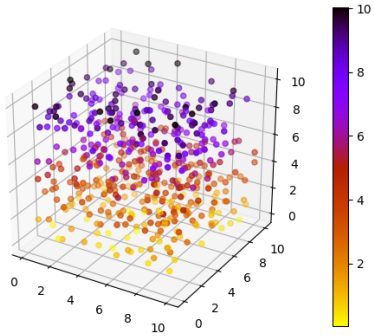

(b)

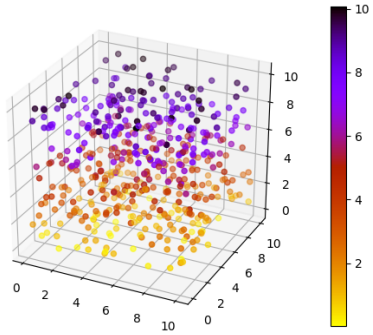

(c)

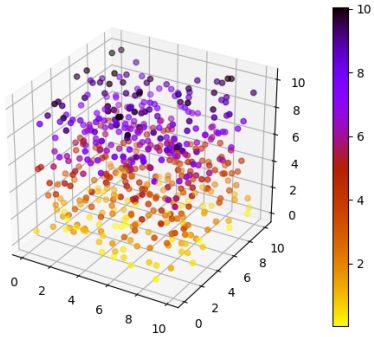

(d) 3D plots of a system of $N = 512$ particles, $T_0 = 1.4$, $\rho = 0.5$ and $n = 6$. (a) $A = 0.0$; (b) $A = 0.75$; (c) $A = 1.5$; (d) $A = 4.0$. Slight coarse-graining is observed for the fluid (b).

Figure 24

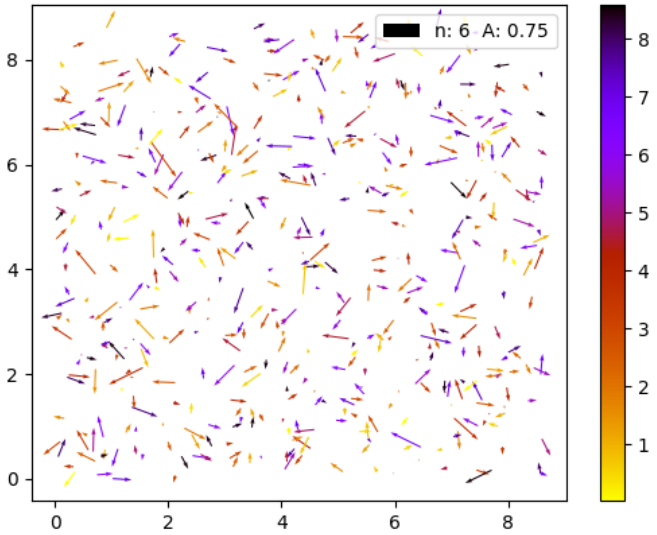

Figure 25: Fluid system with $\rho = 0.8$, $N = 512$, $A = 0.75$, $n = 6$. "Holes" are observed in the fluid stating lack of density.

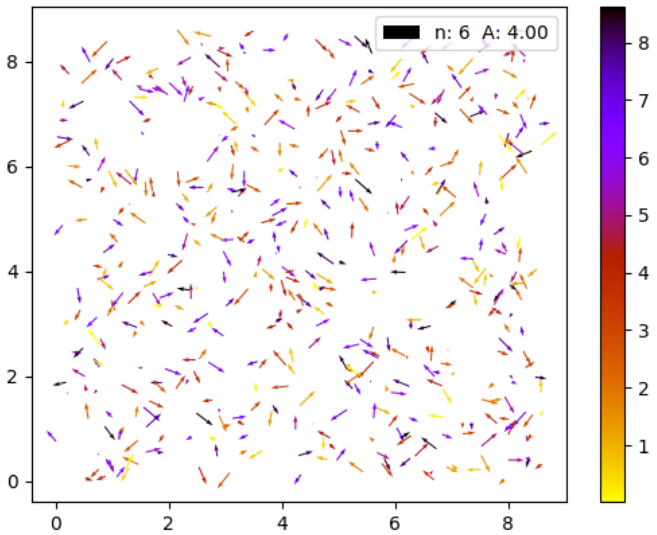

Figure 26: Fluid system with $\rho = 0.8$, $N = 512$, $A = 4.0$,$n = 6$. "Holes" are observed in the fluid stating lack of density.